Naval Research Laboratory

Washington, DC 20375-5000

NRL/FR/5753—92-9371

Nonlinear Modeling of Gated Range Tracker Dynamics with Application to Radar Range Resolution

EYAD H. ABED

Department of Electrical Engineering and the
Systems Research Center
University of Maryland
College Park, MD 20742

ALLEN J. GOLDBERG AND ROBERT E. GOVER

Advanced Techniques Branch
Tactical Electronic Warfare Division

September 22, 1992

REPORT DOCUMENTATION PAGE

Form Approved
OMB No. 0704-0188

1. AGENCY USE ONLY (*Leave Blank*)	2. REPORT DATE	3. REPORT TYPE AND DATES COVERED
	September 22, 1992	Phase I 01 Oct 88 - 30 Sep 89

4. TITLE AND SUBTITLE

Nonlinear Modeling of Gated Range Tracker Dynamics with Application to Radar Range Resolution

5. FUNDING NUMBERS

PE -62113N
57-2595

6. AUTHOR(S)

Eyad H. Abed, Allen J. Goldberg, and Robert E. Gover

7. PERFORMING ORGANIZATION NAME(S) and ADDRESS(ES)

Naval Research Laboratory
Washington, DC 20375-5320

8. PERFORMING ORGANIZATION REPORT NUMBER

NRL/FR/5753—92-9371

9. SPONSORING/MONITORING AGENCY NAME(S) AND ADDRESS(ES)

Office of Chief of Naval Research
800 N. Quincy St.
Arlington, VA 22217-5000

10. SPONSORING/MONITORING AGENCY REPORT NUMBER

11. SUPPLEMENTARY NOTES

Published in January 1991 issue of IEEE Trans. on Aerospace and Electronics Systems. Published in the proceedings of the 29th IEEE conference on Decision & Control, Honolulu, Hawaii, 5-7 Dec 90.

12a. DISTRIBUTION/AVAILABILITY STATEMENT

Approved for public release; distribution unlimited

12b. DISTRIBUTION CODE

13. ABSTRACT (*Maximum 200 words*)

Nonlinear dynamic models for gated radar range trackers are developed and applied to the range resolution problem. Two common types of tracking loop dynamics, as well as the automated gain control (AGC), are accounted for in the models. The null detector is formulated in a general way that encompasses many important error detector laws, including centroid and leading-edge. Both discrete-time and continuous-time dynamic models are presented for each class of tracking loop. The discrete-time models are derived by using an analytical description of the pulse-to-pulse dynamics of the tracker. The continuous-time models are approximations of their discrete-time counterparts for sufficiently small values of the pulse repetition interval. Each of the models is analyzed for a deterministic target return condition. General criteria for asymptotic stability of equilibrium points of the models are studied. The most striking of the stability criteria is a sign requirement on the slope of a "range error curve." These criteria are used in a two-target example to evaluate conclusions on a tracker's resolution capability as a function of target separation. These conclusions are compared with those obtained previously using Woodward's "ambiguity function" approach to resolvability.

14. SUBJECT TERMS

Range gate
Range gate model
Radar dynamics
Tracker dynamics
Range gate stability

15. NUMBER OF PAGES

29

16. PRICE CODE

17. SECURITY CLASSIFICATION OF REPORT	18. SECURITY CLASSIFICATION OF THIS PAGE	19. SECURITY CLASSIFICATION OF ABSTRACT	20. LIMITATION OF ABSTRACT
UNCLASSIFIED	UNCLASSIFIED	UNCLASSIFIED	UL

CONTENTS

NONLINEAR MODELING OF GATED RANGE TRACKER DYNAMICS WITH APPLICATION TO RADAR RANGE RESOLUTION

1. INTRODUCTION

The primary goal of this report is to establish nonlinear dynamic models for an important class of automatic range tracking systems, namely gated range trackers. A second goal is to use the resulting models to gain insight into radar range tracking behavior in multiple-target environments. The class of range trackers addressed in this work includes the "split-gate" system, which involves the generation of two gates, the "early" and the "late" gates. These gates are positioned in time so that a portion of the echo pulse passes through each gate. The tracking system adjusts the split gates so as to drive an associated error voltage to zero [1, pp. 114-115]. The performance of such range tracking systems is well-understood in the single-target environment, but erroneous tracks can result in the presence of interfering targets. Nonlinear dynamic models such as those derived here can be helpful in studying such behavior.

By studying the response of this class of dynamical tracking systems under multiple-target conditions, we hope to identify or characterize the ability of this feedback system to distinguish or resolve individual targets or target groups. For example, if we imagine a situation in which two targets are separating from one another, we are interested in characterizing the tendency of the tracker to focus ultimately on one target in preference to another. This behavior can be thought of as a "resolving capability" or "resolving power" of the tracker, and bears an interesting relationship to the information-theoretic notion of resolvability (which has been discussed at length in other sources [see, for instance, Ref. 2 and references therein, Ref. 3, Chap. 7, and Ref. 4]. Resolving power can be thought of as an ultimate limit based on properties intrinsic to the composite returned signal, as opposed to resolving capability, which concerns the resolving power of an actual tracker. Although the performance of the class of trackers under study may not be optimum, they are nevertheless of considerable interest. In what follows, we use the phrase *resolving power* to describe a property of a particular tracker or class of trackers, while we use the term *resolvability* in referring to properties of the received data itself without regard to the tracker. Note that the term resolving power has also been used to refer to the ability of a lens system to separate images of two objects in close proximity to one another [5, p. 37].

An important benefit of analytical modeling of tracker dynamics is the possibility of predicting track statistics and probability of target selection at formula speeds that are several orders of magnitude faster than currently used pulse-to-pulse simulations. This report lays the foundation for such rapid predictions by setting up a mathematical modeling framework that is amenable to analysis by powerful control systems methods. Although the focus here is on deterministic analysis, the dynamical equations are also valid under conditions of randomly fluctuating signals.

This report follows what can be called a "control systems approach," in the sense that gated range trackers are modeled as nonlinear feedback control systems aiming toward an understanding of nonlinear effects and stability. The first step in this approach is to carefully construct a dynamical model for the range trackers under study. Control systems tools are highly relevant to the study of tracker performance in a multiple target environment. Questions of track point stability (both deterministic and stochastic), probability of tracking a given target, and optimal tracker design are readily posed in the language of control systems. More importantly, once the system dynamic model is constructed, powerful analytical and computational tools from control systems can be applied.

Manuscript approved January 23, 1992.

A major outcome of the present work is a collection of analytical models that are useful in predicting a range tracker's behavior, even when several targets are in the same range gate. These are nonlinear dynamic models given in state space form that summarize the pulse-to-pulse dynamics of the tracker. The nonlinearity of the models is an essential feature, since track points within a range gate are then identified simply as certain *invariant sets* of the appropriate model. We show that track points correspond to *equilibrium points* of the new models if random pulse-to-pulse variation of the received radar signal can be neglected.

To illustrate the potential benefits of our approach, we show interesting new results that provide stability criteria for track points within the same range gate. These criteria can be interpreted as tracker resolving power criteria in range, for targets in one range gate. The criteria are analytical in nature. By considering the results of this paper in the light of resolvability results, one can see how well the tracker performs relative to the theoretical limits.

The remainder of this paper is organized as follows. Section 2 concerns modeling and analysis of the gated range tracker assuming a first-order track loop; Section 3 describes the practically more significant case involving a second-order track loop. Section 2.1 contains the derivation of a novel fourth-order discrete-time model of a gated range tracker (Model DT1). In Section 2.2, stability results for track points assuming this model are derived. Section 2.3 illustrates the application of the results of Sections 2.1 and 2.2 to the centroid problem. Section 2.4 is concerned with the derivation and analysis of a second-order continuous-time model (Model CT1) that approximates Model DT1 when the pulse repetition interval is sufficiently small. The development of Section 3, in which the case of a second-order tracker loop is considered, parallels that of Section 2. In particular, Section 3 contains the derivation of two models, Model DT2 and Model CT2, that are the natural extensions of Models DT1 and CT1, respectively, to the setting of Section 3. Conclusions and some directions for further research are discussed in Section 4.

2. GATED RANGE TRACKER WITH A SINGLE INTEGRATOR IN THE TRACK LOOP

2.1. Discrete-Time Model DT1

Block Diagram and Notation

The block diagram in Fig. 1 is the starting point for the derivation of Model DT1.[1] DT1 is the discrete-time nonlinear gated range tracker model for the case of a single integrator in the track loop. The block diagram includes the essential components of real gated range trackers, with a minimum of complexity. Both the automatic gain control (AGC) system and the null tracker are shown.[2]

The notation of Fig. 1 is as follows. All signals are functions of the *continuous* time t. The signal $E(t)$ is the received sum channel voltage signal analytic envelope after passing through the receiver IF filter but before AGC normalization. The scaled signal $U(t) := g(t)E(t)$ results following passage through the AGC, where $g(t)$ denotes the time-varying AGC gain. In reality, the AGC and the IF filtration are performed by the same receiver stages. For convenience, however, these functions appear separated in the block diagram.

In a tracking radar, the aim of the range tracker is to lock on to and track a target in range, as opposed to obtaining a precise estimate of actual target range. The latter is the function of an instrumentation radar [5, Chap. 3]. The estimate of the target slant range in a tracking radar is therefore referred to here as the estimated *relative range*, and is be denoted by $\rho(t)$ (see Fig. 1).

The quantity $\rho(t)$ is fed back at the end of each epoch to define the time reference for the application of sum and difference weighting patterns to the scaled signal $U(t)$, which results in the sum and difference error detector laws. By a suitable choice of weighting patterns, these functional blocks represent a broad class of range gates, as discussed later in greater detail. The sum detector law provides a measure of signal

[1] DT1 is an abbreviation for Discrete-Time 1.

[2] A simpler model incorporating only the null tracker was presented in 1958 by Amiantov and Tikhonov [6]. There, the emphasis was on the effects of noise, and the model used was first-order and linear.

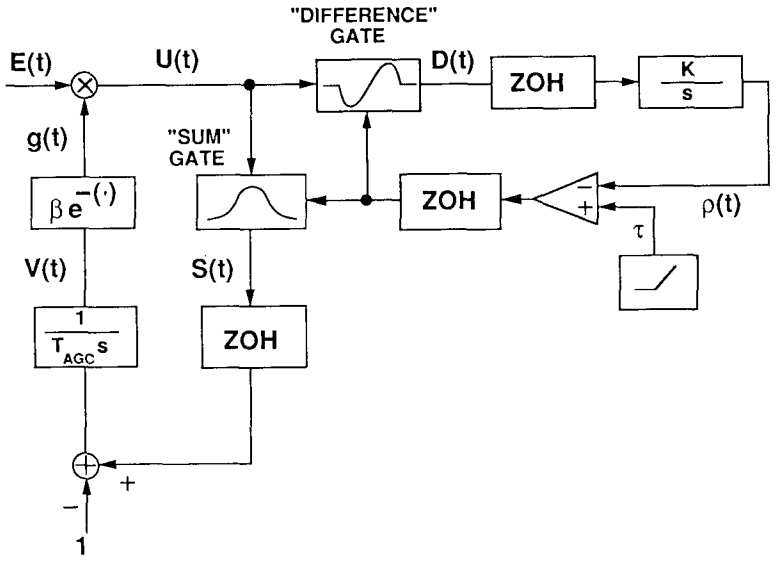

Fig. 1 — Gated range tracker with AGC

strength that drives the AGC; the error detector law senses the "null" of the tracker. The difference, or error, detector law block in Fig. 1 summarizes the effect of the standard range null sensing subsystem. This subsystem consists of an early gate, a late gate, and a comparator [7, Art. 10-31; 1, pp. 114-115]. The postulated equations governing the sum and difference detector blocks are introduced below.

The signal $V(t)$ is the AGC loop voltage, as identified in Fig. 1. The positive constants β, K, and $T_{\rm AGC}$ are, respectively, the (internal) fixed AGC gain, tracker gain, and AGC time constant. Sample-and-hold operations are represented by the symbol ZOH (for zero-order hold), with sampling performed at time instants $t_k = kT_{\rm PRI}$. Here k is any positive integer, and $T_{\rm PRI}$ is the pulse repetition interval (also referred to as interpulse period, epoch length, pulse-to-pulse duration). The ZOH immediately following the sum detector block in Fig. 1 yields as output a measure of overall signal strength that drives the AGC loop; the output of the ZOH following the difference detector is the difference between early and late gate outputs. Each of these ZOH outputs is a constant during any epoch, the value of which is determined by the evolution of the input voltage variables over the immediately preceding epoch, and by the estimated relative range at the conclusion of the that epoch. (This will be made precise in the following.) The appearance of the third ZOH in Fig. 1, following the comparator and preceding the detector blocks, amounts to invoking the following reasonable assumption: The error drive to the detector blocks (i.e., the relative range estimate used as a reference for the kernels in the associated integrations) is updated at the end of each epoch, regardless of the precise pulse arrival time within an epoch.

Analytical modeling of the gated range tracker based directly on the block diagram of Fig. 1 is complicated by the following difficulty. Although we are mainly interested in summarizing the dynamics on a pulse-to-pulse (i.e., discrete-time) basis, Fig. 1 leads to an analog model. Solving this model on a pulse-to-pulse basis is seldom possible (this depends on the detector laws), and even in cases where it is possible, the resulting discrete-time model can be unwieldy. This observation is in part based on lengthy computations that need not be reproduced here.

Two steps are now taken to deal with this difficulty. Typically, the mass of the sum weighting pattern is concentrated in an interval of length much less than the size of the pulse repetition interval $T_{\rm PRI}$. Therefore the AGC gain $g(t)$ does not vary significantly over a single epoch. This is true, even for fast AGC systems. Thus, we can insert an artificial zero-order hold operator following the AGC loop integrator block $((T_{\rm AGC}s)^{-1})$ in the block diagram (see Fig. 2). Next, waveforms are divided into their components during epochs, i.e., for $k = 0, 1, 2, \ldots$, define the kth epoch I_k as

$$I_k := \{t : kT_{\rm PRI} \leq t < (k+1)\, T_{\rm PRI}\}.$$

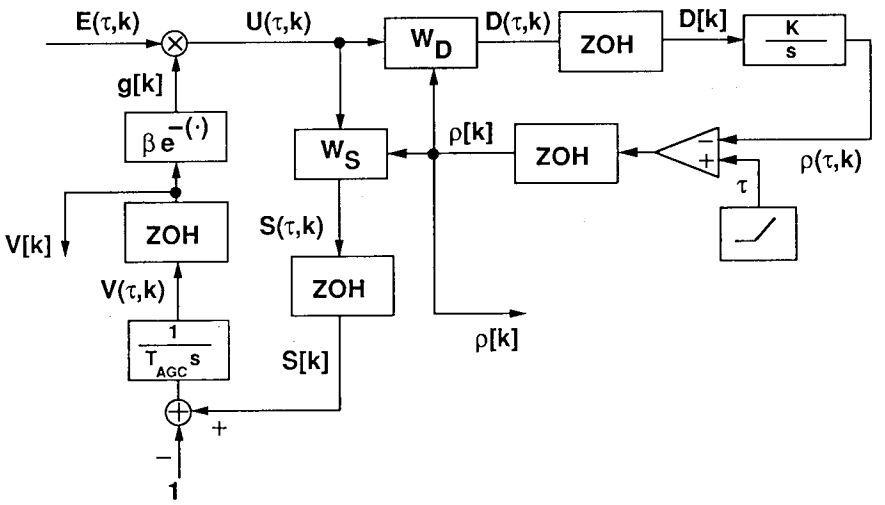

Fig. 2 — Tracker with artificial zero-order-hold

More precisely, for any continuous-time variable $q(t)$, we introduce the notation

$$q(\tau,k) := \begin{cases} q(\tau + (k+0.5)\,T_{\rm PRI}), & \text{for } -T_1 \le \tau < T_1, \\ 0, & \text{otherwise,} \end{cases} \tag{1}$$

for $k = 0, 1, 2, \ldots$, where $T_1 := 0.5\,T_{\rm PRI}$.

The notation introduced in Eq. (1) was chosen to simplify manipulations arising in the following. Regarding this notation, note that the fact that τ can take negative values does not present a problem. Indeed, for $\tau = -T_1$, physical time is given by $t = \tau + (k+0.5)T_{\rm PRI} = kT_{\rm PRI}$, which is never negative. In using this notation, it is convenient to redraw Fig. 1 as in Fig. 2, which is to be construed as depicting Fig. 1 within epoch I_k, modified to include the artificial zero-order hold operator in the AGC loop. The blocks labeled as "sum gate" and "difference gate" in Fig. 1 are now identified as sum and difference detectors W_S and W_D associated with weighting patterns w_S and w_D, respectively.

The following additional notation will be useful. For any variable $q(t)$, and any integer $k \ge 1$, denote by $q[k]$ the value of variable $q(t)$ at the *end* of epoch I_{k-1}. More precisely, $q[k]$ denotes the following limit taken as τ approaches T_1 from the left:

$$\begin{aligned} q[k]: &= \lim_{\tau \uparrow T_1} q(\tau, k-1) \\ &= \lim_{\tau \uparrow T_1} q(\tau + (k-0.5)\,T_{\rm PRI}) \\ &= q((kT_{\rm PRI})^-), \end{aligned} \tag{2}$$

where the superscript "−" signifies that in case the function $q(t)$ has a discontinuity at $t = kT_{\rm PRI}$, we take the limit from the left. For instance, $\rho[k]$ means $\rho((kT_{\rm PRI})^-)$, and $V[k]$ means $V((kT_{\rm PRI})^-)$. This notation will be useful in writing a discrete-time model for the range tracker based on Fig. 2. The notation lends itself to graphical interpretation as in Fig. 3, where a "raster" type of sketch for functions $q(\tau,k)$ is used. In this representation, each epoch corresponds to exactly one raster line. The signals $q(\tau,k)$ vary continuously on the raster lines, while signals $q[k]$ vary discretely and summarize functional values at the *right end points* of the raster lines, with the limit taken as τ increases to its final value T_1 on each raster line.

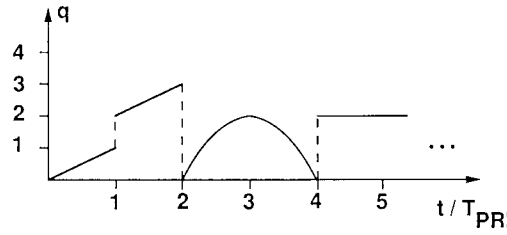

(a) Continuous representation $q(t)$

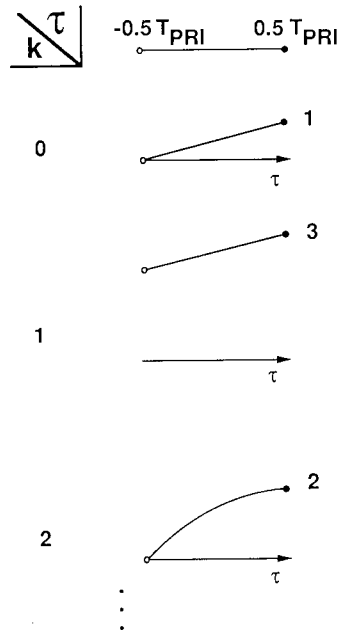

(b) Raster representation $(q(\tau,k)$

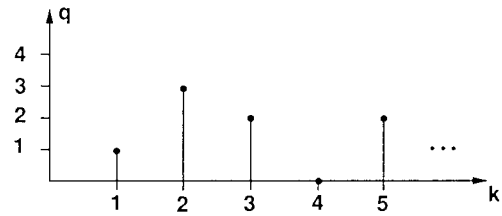

(c) Discrete representation $q[k]$

Fig. 3 — Signal representations

In the following, in keeping with the notation introduced above, the same variable *name* is used for differing *representations* of a signal. The representation used is implied by the manner in which arguments of the signal are denoted. That is, $q(t)$ is always understood to be a *continuous-time signal* with time t being any nonnegative real number; $q(\tau, k)$ is a representation of $q(t)$ in the raster form shown in Fig. 3, and is thus a mixed continuous-discrete representation; and $q[k]$ is a discrete-time signal, obtained by sampling the raster signal $q(\tau, k)$ as discussed above and illustrated in Fig. 3. The following terminology is introduced for the various independent time variables: t is real time, k is epoch time, and τ is intra-epoch time.

Before deriving the desired discrete-time model, the relationships governing the sum and difference detector blocks must be stated. For the sum detector block, denoted W_S in Fig. 2, we have

$$S(\tau, k) = \int_{-T_1}^{\tau} |U(\sigma, k)|^2 \, w_S(\sigma - \rho[k]) \, d\sigma. \tag{3}$$

As for the difference detector block, denoted W_D in Fig. 2, we have

$$D(\tau, k) = \int_{-T_1}^{\tau} |U(\sigma, k)|^2 \, w_D(\sigma - \rho[k]) \, d\sigma. \tag{4}$$

The forms of detector laws given by Eqs. (3) and (4) are very versatile and powerful; a wide variety of systems can be modeled by adopting suitable sum and difference kernels (weighting patterns) w_S and w_D. For example, when w_S is chosen to be an even pattern, and w_D an odd pattern (as depicted in Fig. 4). then detectors of Eqs. (3) and (4) implement a common form of centroid tracker. The shape of w_S determines the range gate width or aperture. In common radar terminology, the lobe occurring for σ negative in Fig. 4d represents the "early gate," and, likewise, the lobe for σ positive is called the "late gate."

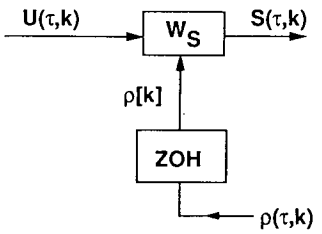

(a) "Sum" detector subsystem

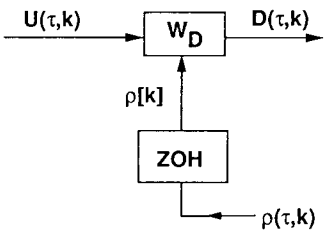

(b) "Difference" detector subsystem (early and late gates)

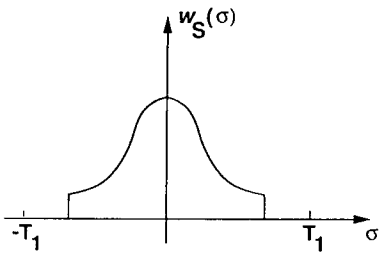

(c) Generic sum weighting pattern

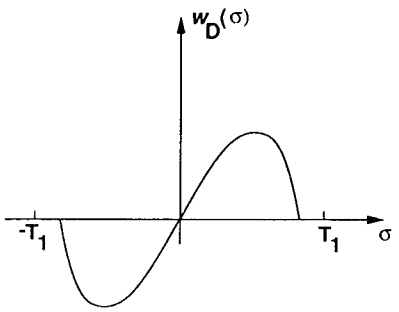

(d) Generic difference weighting pattern

Fig. 4 — Detector Laws

According to Eqs. (2), (3), and (4), the discrete-time variables $S[k]$, $D[k]$ are given by

$$S[k] = \int_{-T_1}^{T_1} |U(\sigma, k-1)|^2 \, w_S(\sigma - \rho[k-1]) \, d\sigma, \tag{5}$$

$$D[k] = \int_{-T_1}^{T_1} |U(\sigma, k-1)|^2 \, w_D(\sigma - \rho[k-1]) \, d\sigma. \tag{6}$$

Equations (5) and (6) prove useful in the model derivation, which is pursued next.

Derivation of Model DT1

With notation now established, we proceed with the derivation of a model in state equation form describing the discrete-time dynamics of Fig. 2. The variables of most interest in Fig. 2 are the relative slant range estimate $\rho[k]$ and the AGC voltage $V[k]$. Figure 2 can be used to write dynamical equations satisfied by these variables.

For instance, it is clear from the block diagram that

$$\begin{aligned} U(\tau, k) &= E(\tau, k) \, g[k] \\ &= \beta E(\tau, k) e^{-V[k]}. \end{aligned} \tag{7}$$

Also, from the $(T_{\mathrm{AGC}} s)^{-1}$ integrator block, accounting for the fact that $V[k]$ is the initial value of $V(\tau, k)$ at the beginning of the kth epoch and noting the effect of the zero-order hold following W_S in Fig. 2, we have

$$\begin{aligned} V(\tau, k) &= \lim_{\sigma \uparrow T_1} \{V(\sigma, k-1)\} + \frac{1}{T_{\mathrm{AGC}}} \int_{-T_1}^{\tau} (S[k] - 1) \, d\sigma \\ &= V[k] + \frac{\tau + T_1}{T_{\mathrm{AGC}}} (S[k] - 1). \end{aligned} \tag{8}$$

Therefore,

$$\begin{aligned} V[k+1] &= \lim_{\tau \uparrow T_1} V(\tau, k) \\ &= V[k] + \frac{T_{\mathrm{PRI}}}{T_{\mathrm{AGC}}} (S[k] - 1). \end{aligned} \tag{9}$$

Now, Eqs. (5) and (7) imply that $S[k]$ is given by

$$\begin{aligned} S[k] &= \int_{-T_1}^{T_1} |U(\sigma, k-1)|^2 \, w_S(\sigma - \rho[k-1]) \, d\sigma \\ &= \beta^2 e^{-2V[k-1]} \int_{-T_1}^{T_1} |E(\sigma, k-1)|^2 \, w_S(\sigma - \rho[k-1]) \, d\sigma. \end{aligned} \tag{10}$$

Equation (10) is now substituted in Eq. (9), yielding

$$V[k+1] = V[k] + \frac{T_{\mathrm{PRI}}}{T_{\mathrm{AGC}}} \left(\beta^2 e^{-2V[k-1]} \int_{-T_1}^{T_1} |E(\sigma, k-1)|^2 w_S(\sigma - \rho[k-1]) \, d\sigma - 1 \right). \tag{11}$$

Similarly, Eqs. (6) and (7) imply that $D[k]$ is given by

$$\begin{aligned} D[k] &= \int_{-T_1}^{T_1} |U(\sigma, k-1)|^2 \, w_D(\sigma - \rho[k-1]) \, d\sigma \\ &= \beta^2 e^{-2V[k-1]} \int_{-T_1}^{T_1} |E(\sigma, k-1)|^2 \, w_D(\sigma - \rho[k-1]) \, d\sigma. \end{aligned} \tag{12}$$

From the blocks in Fig. 2 corresponding to the tracker, we obtain

$$\rho(\tau, k) = \rho[k] + K(\tau + T_1) \, D[k]. \tag{13}$$

Taking $\lim_{\tau \uparrow T_1}$ of Eq. (13) gives

$$\rho[k+1] = \rho[k] + K T_{\text{PRI}} \, D[k]. \tag{14}$$

Using Eqs. (12) in (14) now yields

$$\rho[k+1] = \rho[k] + K\beta^2 \, T_{\text{PRI}} e^{-2V[k-1]} \int_{-T_1}^{T_1} |E(\sigma, k-1)|^2 \, w_D(\sigma - \rho[k-1]) \, d\sigma. \tag{15}$$

Equations (11) and (15) are a coupled pair of second-order difference equations for the variables $V[k]$ and $\rho[k]$. For ease of reference, these two equations are collected to form the first representation of the dynamics of the range tracker of Fig. 2:

$$\rho[k+1] = \rho[k] + K\beta^2 \, T_{\text{PRI}} e^{-2V[k-1]} \int_{-T_1}^{T_1} |E(\sigma, k-1)|^2 \, w_D(\sigma - \rho[k-1]) \, d\sigma, \tag{16a}$$

$$V[k+1] = V[k] + \frac{T_{\text{PRI}}}{T_{\text{AGC}}} \left(\beta^2 e^{-2V[k-1]} \int_{-T_1}^{T_1} |E(\sigma, k-1)|^2 \, w_S(\sigma - \rho[k-1]) \, d\sigma - 1 \right). \tag{16b}$$

Equation (16) is a self-contained description of the evolution of the variables $\rho[k]$, $V[k]$, and its solution requires knowledge only of the initial conditions on these variables and of the received signal $E(\tau, k)$.

For many considerations, including those related to questions of stability, it is often useful to recast difference equation models such as Eq. (16) in the so-called state space form. In this form, only first-order difference equations appear. To derive a state space representation from Eq. (16), we introduce unit-delayed signals associated with $\rho[k]$ and $V[k]$. These are given by

$$\rho_d[k] := \rho[k-1] \tag{17a}$$

and

$$V_d[k] := V[k-1], \tag{17b}$$

respectively. Model DT1 is given by the following system of four first-order difference equations. This is a state space representation for the dynamics of Fig. 2 and is indeed equivalent to the pair (Eq. (16)) of second-order difference equations.

Model DT1:

$$\rho[k+1] = \rho[k] + K\beta^2 \, T_{\text{PRI}} e^{-2V_d[k]} \int_{-T_1}^{T_1} |E(\sigma, k-1)|^2 \, w_D(\sigma - \rho_d[k]) \, d\sigma \tag{18a}$$

$$\rho_d[k+1] = \rho[k] \tag{18b}$$

$$V[k+1] = V[k] + \frac{T_{\text{PRI}}}{T_{\text{AGC}}} \left(\beta^2 e^{-2V_d[k]} \int_{-T_1}^{T_1} |E(\sigma, k-1)|^2 \, w_S(\sigma - \rho_d[k]) \, d\sigma - 1 \right) \tag{18c}$$

$$V_d[k+1] = V[k]. \tag{18d}$$

Equation (18) is the desired four-dimensional discrete-time model describing the gated range tracker for the case of a single integrator in the track loop. The model is written in state equation form, with state vector $(\rho[k],\ \rho_d[k],\ V[k],\ V_d[k])$.

It is important to note that the echo return signal E has been treated in a very general way in the derivation of this model, which allows both deterministic and stochastic signals E. In the case of a stochastic return signal, E in Eq. (18) is a stochastic process, the outputs of the error-detector laws are stochastic processes, and the Model DT1 should be treated as a system of stochastic difference equations.

In the next section, this model is used to derive criteria for deterministic stability of track points in a fixed range gate.

2.2. Track Points and Stability of Model DT1

Intuitively, we might expect that track points of the gated range tracker of Fig. 2 correspond to equilibrium points of Model DT1.[3] In reality, however, Eq. (18) may fail to have equilibrium points because of the (random) variation of the received radar signal $E(\sigma, k-1)$ between epochs. Track points can then be thought of as trajectories of the Model DT1 in which $\rho[k]$ = a constant = $\rho_d[k]$, but $V[k]$ is allowed to vary with $E(\sigma, k-1)$. These trajectories, when they exist, are invariant sets of Eq. (18). To simplify the analysis below, it is assumed that the received signal E has no pulse-to-pulse variation. Under this assumption, track points can be identified with equilibrium points of Eq. (18). First, the equations for an equilibrium are derived.

At an equilibrium point of DT1, if one exists, we require $\rho[k+1] = \rho[k]$, $\rho_d[k+1] = \rho_d[k]$, $V[k+1] = V[k]$, and $V_d[k+1] = V_d[k]$. Referring to Eq. (18), it follows that an equilibrium $(\rho^*, \rho_d^*, V^*, V_d^*)$ satisfies

$$\rho^* = \rho_d^*, \tag{19a}$$

$$V^* = V_d^*, \tag{19b}$$

as well as

$$\int_{-T_1}^{T_1} |E(\sigma, k-1)|^2 \, w_D(\sigma - \rho^*) d\sigma = 0, \tag{19c}$$

$$\beta^2 e^{-2V^*} \int_{-T_1}^{T_1} |E(\sigma, k-1)|^2 \, w_S(\sigma - \rho^*) d\sigma - 1 = 0. \tag{19d}$$

To solve for an equilibrium, we first solve Eq. (19c) for ρ^*, giving, perhaps, multiple solutions. Next, these values are substituted for ρ^* in Eq. (19d), and we attempt to solve for the equilibrium voltage V^*.

If the only variation in E between epochs is a scaling of some base waveform, then Fig. 4d indicates that a solution of Eq. (19c) for ρ^* may exist. However, in this case Eq. (19d) will not be solvable for V^*. Thus, the relative slant range may in principle be estimated without convergence of the AGC. This is an example of a track point that is not an equilibrium point of Eq. (18).

Now assume that the received pulses in all epochs are identical waveforms. Then $E(\tau, k)$ is independent of k, and we can write

$$\begin{aligned} E(\tau, k) &= E(\tau, 0) \text{ for all } \tau, k \\ &=: E_0(\tau). \end{aligned} \tag{20}$$

[3] An *equilibrium point* (or *fixed point*) of a discrete-time system $x[k+1] = f(x[k])$ is defined as a vector ξ for which $\xi = f(\xi)$.

Equations (19c), (19d) for an equilibrium can now be simplified to yield

$$F_D(\rho^*) = 0 \tag{21a}$$

$$\beta^2 e^{-2V^*} F_S(\rho^*) - 1 = 0, \tag{21b}$$

where $F_D(\rho)$ is the *range error function*

$$F_D(\rho) := \int_{-T_1}^{T_1} |E_0(\sigma)|^2 \, w_D(\sigma - \rho) \, d\sigma, \tag{22a}$$

and $F_S(\rho)$ is defined as

$$F_S(\rho) := \int_{-T_1}^{T_1} |E_0(\sigma)|^2 \, w_S(\sigma - \rho) \, d\sigma. \tag{22b}$$

With the assumption of Eq. (20), it is clear from Fig. 4 and Eq. (21) that equilibria will typically exist, and that the number of equilibria depends on the waveform $E_0(\tau)$ and the null detector curve $w_D(\sigma)$. Moreover, since Eq. (21b) can have no more than a single solution for V^* corresponding to a given value of ρ^*, it follows that track points can be identified with equilibrium points when Eq. (20) holds.

It is interesting to note that if the received pulses are identical up to a time shift, as in Eq. (20), the dynamical equations (18) are autonomous. That is, $E_0(\tau)$ does not appear as an external input, but rather as an integral part of the dynamics. Only pulse-to-pulse variations in $E(\tau, k)$ (i.e., variation of $E(\tau, k)$ with k) could represent external inputs to the model.

To study equilibrium point stability under the assumption of Eq. (20), it is convenient to rewrite the model (Eq. (18)) in the light of Eq. (20) and the notation introduced by Eq. (22). We have

Model DT1 for Periodic Received Waveform:

$$\rho[k+1] = \rho[k] + K T_{\mathrm{PRI}} \, \beta^2 e^{-2V_d[k]} F_D(\rho_d[k]) \tag{23a}$$

$$\rho_d[k+1] = \rho[k] \tag{23b}$$

$$V[k+1] = V[k] + \frac{T_{\mathrm{PRI}}}{T_{\mathrm{AGC}}} \left(\beta^2 e^{-2V_d[k]} \, F_S(\rho_d[k]) - 1\right) \tag{23c}$$

$$V_d[k+1] = V[k]. \tag{23d}$$

The Jacobian matrix of Eq. (23) evaluated at an equilibrium, denoted J, is given by

$$J := \begin{pmatrix} 1 & a & 0 & 0 \\ 1 & 0 & 0 & 0 \\ 0 & b & 1 & c \\ 0 & 0 & 1 & 0 \end{pmatrix}. \tag{24}$$

where the scalars a, b, c are defined as follows (here a prime denotes differentiation with respect to the argument of a function):

$$a := K\beta^2 \, T_{\mathrm{PRI}} e^{-2V^*} F_D'(\rho^*), \tag{25a}$$

$$b := \frac{\beta^2 \, T_{\mathrm{PRI}} e^{-2V^*}}{T_{\mathrm{AGC}}} F_S'(\rho^*), \tag{25b}$$

$$c := \frac{-2\beta^2 \, T_{\mathrm{PRI}} e^{-2V^*}}{T_{\mathrm{AGC}}} F_S(\rho^*). \tag{25c}$$

A classical stability theorem [8, Appendix A] implies that the equilibrium $(\rho^*, \rho^*, V^*, V^*)$ is asymptotically stable if each eigenvalue of J lies (strictly) within the unit circle in the complex plane. If any eigenvalue has magnitude greater than unity, the equilibrium is unstable.[4]

The matrix J is seen to be block lower triangular, so that its eigenvalues are those of the lower right and upper left 2×2 blocks. The characteristic polynomial of the lower right block is

$$p_1(\lambda) := \lambda^2 - \lambda + \frac{2\beta^2 T_{\mathrm{PRI}} e^{-2V^*}}{T_{\mathrm{AGC}}} F_S(\rho^*), \tag{26}$$

while that of the upper left block is

$$p_2(\lambda) := \lambda^2 - \lambda - K\beta^2 T_{\mathrm{PRI}} e^{-2V^*} F_D'(\rho^*). \tag{27}$$

Determination of conditions for stability of these characteristic polynomials is facilitated by the following result (see, for instance, Ref. 8).

Lemma 1 (Jury's Test for Second-Order Systems). *A necessary and sufficient condition for the zeros of the polynomial*

$$p(\lambda) = a_2\lambda^2 + a_1\lambda + a_0 \tag{28}$$

$(a_2 > 0)$ to lie within the unit circle is

$$p(1) > 0, \tag{29a}$$

$$p(-1) > 0, \text{and} \tag{29b}$$

$$|a_0| < a_2. \tag{29c}$$

Applying Lemma 1 to $p_1(\lambda)$, we see that Eqs. (29a) and (29b) are trivially satisfied due to the positivity of $|E_0(\sigma)|$ and $w_S(\sigma - \rho^*)$ (see Fig. 4), and that Eq. (29c) is equivalent to

$$\frac{2\beta^2 T_{\mathrm{PRI}} e^{-2V^*}}{T_{\mathrm{AGC}}} F_S(\rho^*) < 1. \tag{30}$$

The equations for an equilibrium allow simplification of Eq. (30) to

$$T_{\mathrm{AGC}} > 2T_{\mathrm{PRI}}. \tag{31}$$

Equation (31) is usually satisfied in practical systems, so that it does not represent a critical test for stability. However, it is interesting to note that Eq. (31) does represent a necessary condition for the existence of at least one stable equilibrium point under the assumption of a periodic received signal: The AGC loop time constant must be greater than twice the length of the pulse repetition interval.

Applying Lemma 1 to the polynomial $p_2(\lambda)$, we find that Eq. (29a) asserts

$$F_D'(\rho^*) < 0, \tag{32}$$

and that this implies Eq. (29b) for $p_2(\lambda)$. Equation (29c) is found to assert

$$\frac{|F_D'(\rho^*)|}{F_S(\rho^*)} < (K\ T_{\mathrm{PRI}})^{-1}. \tag{33}$$

[4] Cases in which at least one eigenvalue lies on the unit circle are known as *critical cases* in stability. These require nonlinear analysis to determine even the local stability properties. Note that arbitrary small perturbations in the model force critical eigenvalues off the unit circle. Hence, if a robust form of asymptotic stability is desired, it is necessary and sufficient that all the eigenvalues lie within the unit circle.

Combining Eqs. (32) and (33) gives the requirement

$$0 < -F'_D(\rho^*) < (K\,T_{\mathrm{PRI}})^{-1}\,F_S(\rho^*). \tag{34}$$

Satisfying Eqs. (31) and (34) guarantees the asymptotic stability of the equilibrium point $(\rho^*, \rho_d^*, V^*, V_d^*) = (\rho^*, \rho^*, V^*, V^*)$ of Eq. (18). Put another way, this equilibrium point is stable if the following three conditions are satisfied:

$$F'_D(\rho^*) < 0, \tag{C1}$$

$$KT_{\mathrm{PRI}} + \frac{F_S(\rho^*)}{F'_D(\rho^*)} < 0, \tag{C2}$$

$$T_{\mathrm{AGC}} > 2T_{\mathrm{PRI}}. \tag{C3}$$

This form of the stability conditions is easily checked to be equivalent to Eqs. (31) and (34). Considering the shape of the null detector curve $w_D(\sigma)$ depicted in Fig. 4(d), condition (C1) on the slope of the range error curve explicates various observations (e.g., Ref. 9) regarding the relationship of closeness of targets: their relative radar cross sections; and the tendency of the range tracker to lock on to either of them, or on to an artificial track point (centroid).

The next theorem summarizes these remarks.

Theorem 1 (Track Point Stability: Model DT1). *Under assumption of Eq.* (20), *the equilibrium point* $(\rho^*, \rho_d^*, V^*, V_d^*) = (\rho^*, \rho^*, V^*, V^*)$ *of Eq.* (18) *is asymptotically stable by the linear approximation if and only if* (C1), (C2), *and* (C3) *hold.*

Condition (C2) may be construed simply as providing an upper bound on the tracker gain K, which is achievable by appropriate choices of tracker parameters. Similarly, (C3) is a blanket condition that must be satisfied, even for the simplest case of a single target present, for stable tracking to be possible. Hence, a track point for which only (C1) holds might still be thought of as resolvable in the sense that a modification in tracker parameters would ensure satisfaction of (C2) and (C3) as well as (C1).

2.3. Two-Target Example using Model DT1

A simple illustration of Theorem 1 is now given. Let $E_0(\sigma)$ consist of a pair of separated but identical triangular pulses, corresponding to two point scatterers in a single range gate. The same example is treated in Burdic [10, Sec. 5.2.1] by using Woodward's [3] autocorrelation-based ambiguity function range-resolution index. The triangular pulse shape reflects the effect of convolution of the IF matched filter impulse response with an assumed rectangular pulse shape of the received signal. As shown in Fig. 5, the targets have delays r_0 and $r_0 + \mu$, respectively. For simplicity, suppose the pulses each have amplitude unity, that they have zero relative phase, and that each has a pulse width T_p. Theorem 1 can be used to study track points and their stability as a function of the parameter μ, the separation between the targets. For the current illustration, stability is examined in detail only for the centroid target. Thus, the conclusions reached concern the possibility that the tracker converges on this false target. This possibility undermines the ability of the range tracker to resolve the actual targets. Figure 6 shows the assumed forms of the sum and difference weighting patterns w_S and w_D, respectively. As is clear from the figure, the weighting patterns are assumed to be nonzero over a range of length precisely T_p. In addition, it is natural to assume that (C3) holds, i.e., that $T_{\mathrm{AGC}} > 2T_{\mathrm{PRI}}$.

By using Eqs. (21a), (21b) for an equilibrium, we find that only two equilibrium points occur for $\mu > 2T_p$. These correspond to the actual targets, and therefore have delays $\rho_1^* = r_0$ and $\rho_2^* = r_0 + \mu$, respectively. To

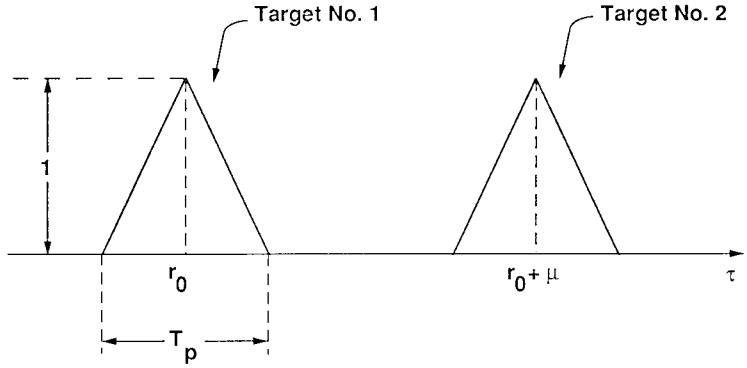

Fig. 5 — Two identical point targets with rectangular envelope and separation $\mu > T_p$

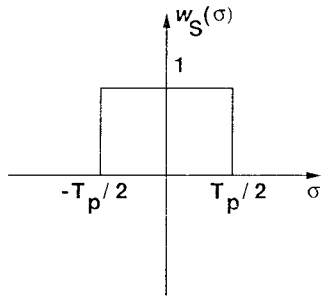

(a) Sum detector law

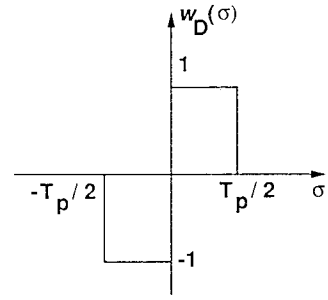

(b) Difference detector law

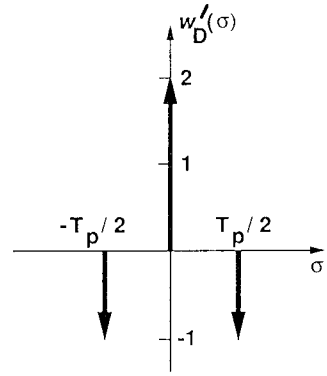

(c) $w_D'(\sigma) = 2\delta(\sigma) - \delta(\sigma - T_p/2) - \delta(\sigma + T_p/2)$

Fig. 6 — Detector laws for example of Section 2.3

study the stability of these equilibria, we apply Theorem 1. Condition (C1) holds for both ρ_1^* and ρ_2^*. This can be seen by noting that

$$w_D\prime(\sigma) = 2\delta(\sigma) - \delta\left(\sigma - \frac{T_p}{2}\right) - \delta\left(\sigma + \frac{T_p}{2}\right) \tag{35}$$

(see Fig. 6(c)), so that, for $\mu > 2T_p$,

$$F_D'(\rho_i^*) = -\int_{-T_1}^{T_1} |E_0(\sigma)|^2 \, w_D'(\sigma - \rho_i^*) \, d\sigma = -2 \tag{36}$$

for $i = 1, 2$. Condition (C2) simplifies to

$$K < \frac{T_p}{6T_{\text{PRI}}}. \tag{37}$$

Hence, the targets are resolved for delays $\mu > 2T_p$ if the tracker gain K is bounded as in Eq. (37).

As μ is decreased below $2T_p$, we expect the appearance of a "centroid track point" at a delay ρ_3^* between the estimated relative ranges ρ_1^* and ρ_2^* of the actual targets. We would expect the centroid to be initially unstable, achieving stability as the separation μ between the targets is made smaller. Theorem 1 is now used to quantify this intuition, and indeed to specify the separation μ_c below which the centroid is stable. The importance of this question stems from the fact that the centroid track point acquires stability only at the expense of the degree to which the tracker can resolve the actual targets.

The centroid track point appears as μ is decreased below $2T_p$. The delay corresponding to this track point is, by symmetry, given by

$$\rho_3^* = r_0 + \frac{\mu}{2}. \tag{38}$$

See Fig. 7. The reason that the centroid track point does not occur for $\mu > 2T_p$ is simply that there would then be no overlap between the weighting pattern $w_S(\sigma - \rho_3^*)$ and $E_0(\sigma)$. Equation (21b) for an equilibrium would then be unsolvable for the AGC voltage V^*. For the situation depicted in Fig. 7. it is easy to check that (C1) is not satisfied, implying instability of the centroid. Thus, the centroid can be stable only if the triangular pulses overlap, which occurs for $\mu < T_p$. Moreover, (C1) must be satisfied for sufficiently small μ. as can be seen by noting that for $\mu = 0$ the centroid and the two targets coincide. Hence. the centroid is a stable track point for a sufficiently small target separation.

As μ is decreased below T_p, the quantity on the left side of (C1) (the slope of the range error curve at the centroid) decreases monotonically. The centroid becomes stable at the critical value $\mu = \mu_c$ for which this quantity vanishes. Denoting by $P(\sigma)$ the triangular pulse waveform shown in Fig. 8. it follows that μ_c is the solution to

$$8P^2(\sigma - r_0)|_{\sigma = r_0 + \frac{\mu}{2}} = 2P^2(\sigma - r_0)|_{\sigma = r_0 + \frac{\mu}{2} - \frac{T_p}{2}} \tag{39}$$

satisfying $\mu < T_p$. Equation (39) simplifies to

$$4P^2\left(\frac{\mu}{2}\right) = P^2\left(\frac{\mu - T_p}{2}\right). \tag{40}$$

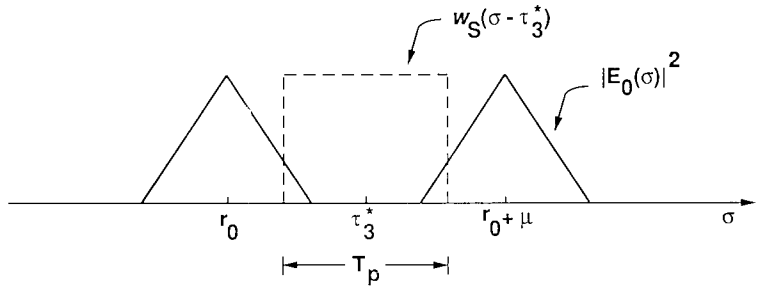

(a) Illustrating overlapping curves $w_S(\sigma - \tau_3^*)$ and $|E_0(\sigma)|^2$

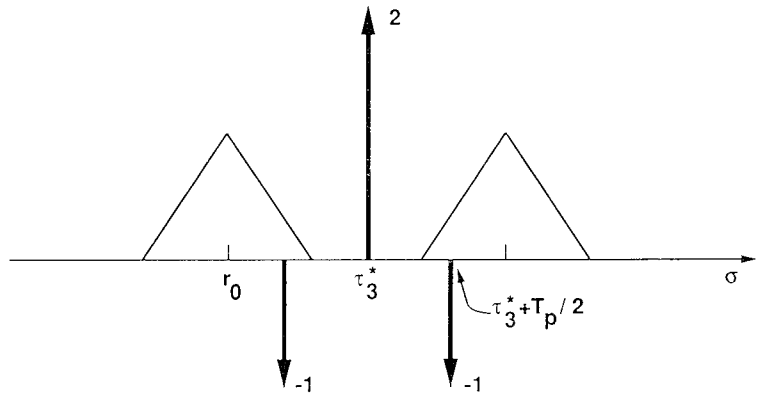

(b) Checking condition (C1)

Fig. 7 — Appearance of centroid track point ($\mu < T_p$)

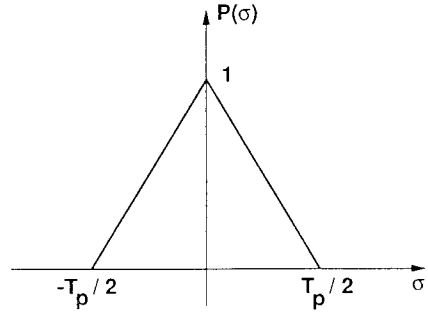

Fig. 8 — Triangular pulse of duration T_p

By using the graph of $P(\sigma)$ depicted in Fig. 8, this can be rewritten as

$$4\left(\frac{4}{T_p^2}\right)\left(\frac{\mu - T_p}{2}\right)^2 = \left(\frac{4}{T_p^2}\right)\left(\frac{\mu}{2}\right)^2, \tag{41}$$

which can be simplified to

$$\frac{3}{4}\left(\frac{\mu}{T_p}\right)^2 - 2\left(\frac{\mu}{T_p}\right) + 1 = 0. \tag{42}$$

Solving Eq. (42) and disregarding the solution with $\frac{\mu}{T_p} > 1$, we obtain

$$\mu_c = \frac{2}{3}\, T_p. \tag{43}$$

Hence, the centroid track point is stable for target separations smaller than two-thirds of the pulse width, but is unstable for greater separations. It is interesting to compare this result with that obtained by Burdic [10, Sec. 5.2.1] using Woodward's approach. There it was concluded that resolution would be achievable only "with great difficulty" (if at all) for separations less than Woodward's time resolution constant, which for this case happens to coincide exactly with the figure derived above: $\frac{2}{3}T_p$. We emphasize that this apparent numerical agreement between the results of the two approaches does not imply that the same conclusion is reached. The approach presented here results in a definite yes or no conclusion on resolving power of the range tracker for any target separation, whereas Woodward's approach gives a somewhat vague statement of relative resolvability. (The vagueness of the conclusions reached by using ambiguity functions was a weakness acknowledged by Woodward [3], and was the primary motivation for subsequent work in resolvability.)

2.4. Approximate Continuous-Time Model CT1

Derivation of Model CT1

The discrete-time model of Eq. (18) studied in the foregoing admits a lower order continuous-time approximation, under the assumption that the size T_{PRI} of the pulse repetition interval is very small in relation to other model parameters. In this section, a pair of first-order ordinary differential equations approximating the model (Eq. (18)) is given and briefly studied under this assumption. It is convenient to focus on the representation of Eq. (16) in terms of a coupled pair of second-order difference equations (this is equivalent to Eq. (18)).

Equation (16) is rewritten in the form

$$\left(\frac{\rho[k+1] - \rho[k]}{T_{\mathrm{PRI}}}\right) = K\beta^2 e^{-2V[k-1]} \int_{-T_1}^{T_1} |E(\sigma, k-1)|^2\, w_D(\sigma - \rho[k-1])\, d\sigma, \tag{44a}$$

$$T_{\mathrm{AGC}}\left(\frac{V[k+1] - V[k]}{T_{\mathrm{PRI}}}\right) = \beta^2 e^{-2V[k-1]} \int_{-T_1}^{T_1} |E(\sigma, k-1)|^2\, w_S(\sigma - \rho[k-1])\, d\sigma - 1. \tag{44b}$$

The terms in braces on the left sides of Eqs. (44a) and (44b) approximate derivatives with respect to time t of the associated continuous-time functions, for sufficiently small values of T_{PRI}. To see this, recall that for any continuous-time signal $q(t)$, the associated discrete-time signal $q[k]$ is obtained by a procedure by which $q(t)$ is sampled with a sampling interval of length T_{PRI}. Replacing the terms in braces by time derivatives and expressing the right sides of Eqs. (44a) and (44b) in terms of the original continuous-time signals yields a continuous-time model. Note that this is *not* the same as taking $\lim_{T_{\mathrm{PRI}} \to 0}$ of Eqs. (44a) and (44b). Indeed, the result of such an operation would be meaningless, considering that the continuous-discrete received signal $E(\tau, k)$ also depends on the parameter T_{PRI}, and this dependence is such that the limit as $\lim_{T_{\mathrm{PRI}} \to 0}$ would not be well defined.

To proceed, suppose real time t is related to epoch time k by the approximate formula $t \approx kT_{\mathrm{PRI}}$. Then the left sides of Eqs. (44a) and (44b) are approximately $\frac{d\rho(t)}{dt}$ and $T_{\mathrm{AGC}}\frac{dV(t)}{dt}$, respectively. The quantities $V[k-1]$, $\rho[k-1]$ appearing in the right sides of Eqs. (44a) and (44b) can be replaced by the continuous-time functions $V(t)$, $\rho(t)$, respectively. Finally, use Eq. (1) to get $E(\sigma, k-1) = E(\sigma + (k-1)T_{\mathrm{PRI}})$ for $0 \le \sigma < T_{\mathrm{PRI}}$. This inequality is clearly satisfied by σ in the integrations of Eq. (44). Therefore, approximate $E(\sigma, k-1)$ in Eq. (44) by $E(\sigma - T_{\mathrm{PRI}} + [\frac{t}{T_{\mathrm{PRI}}}]T_{\mathrm{PRI}})$. The resulting continuous-time model is

Model CT1:

$$\frac{d\rho(t)}{dt} = K\beta^2 e^{-2V(t)} \int_{-T_1}^{T_1} \left| E\left(\sigma - T_{\mathrm{PRI}} + \left[\frac{t}{T_{\mathrm{PRI}}}\right] T_{\mathrm{PRI}}\right)\right|^2 w_D(\sigma - \rho(t))\, d\sigma, \tag{45a}$$

$$T_{\mathrm{AGC}}\frac{dV(t)}{dt} = \beta^2 e^{-2V(t)} \int_{-T_1}^{T_1} \left| E\left(\sigma - T_{\mathrm{PRI}} + \left[\frac{t}{T_{\mathrm{PRI}}}\right] T_{\mathrm{PRI}}\right)\right|^2 w_S(\sigma - \rho(t))\, d\sigma - 1, \tag{45b}$$

where the standard notation $[x]$ is used to denote, for a real number x, the greatest integer less than or equal to x. Equation (45) is the continuous-time model approximating the original discrete-time model (Eq. (16)) (equivalently Eq. (18)). We refer to this model as Model CT1. Note that Eq. (45) is a second-order differential model, whereas the original discrete-time model is fourth-order. Note also that Eq. (45) can represent either an ordinary differential system or a stochastic differential system, corresponding to the statistical character assumed of the target return signal E.

Next we extract from Eq. (45) a differential model corresponding to the discrete-time model (Eq. (23)), which applies in case the received pulses in all epochs are identical waveforms. Assume that $E(t)$ is periodic with period T_{PRI}. Then Eq. (45) becomes

Model CT1 for Periodic Received Waveform:

$$\frac{d\rho(t)}{dt} = K\beta^2 e^{-2V(t)} \int_{-T_1}^{T_1} |E_0(\sigma)|^2\, w_D(\sigma - \rho(t))\, d\sigma, \tag{46a}$$

$$T_{\mathrm{AGC}}\frac{dV(t)}{dt} = \beta^2 e^{-2V(t)} \int_{-T_1}^{T_1} |E_0(\sigma)|^2\, w_S(\sigma - \rho(t))\, d\sigma - 1, \tag{46b}$$

where the notation $E_0(\sigma)$ (in favor of $E(\sigma)$) has been used in analogy with the discrete-time case. It is straightforward to rewrite Eq. (46) in terms of the notation $F_D(\rho(t))$, $F_S(\rho(t))$.

Stability Analysis for Model CT1

Stability of equilibria for the deterministic continuous-time model (Eq. (46)) is now considered briefly. An equilibrium point (ρ^*, V^*) of Eq. (46) solves the same pair of algebraic equations (21) that arise in the discrete-time setting. Stability of an equilibrium is now ascertained by verifying that the eigenvalues of the Jacobian matrix of Eq. (46) at the equilibrium have negative real parts. This Jacobian matrix, also denoted J, is given by

$$J := T_{\mathrm{PRI}}^{-1} \begin{pmatrix} a & 0 \\ b & c \end{pmatrix}, \tag{47}$$

where the scalars a, b, c are as defined in Eq. (25). Since J is triangular, its eigenvalues are identical to its diagonal elements a and c, both of which are real. It is easy to see that a is negative precisely when (C1) holds, and that c is ensured negative by the positivity of the sum weighting pattern w_S. Hence (C1) is sufficient for stability of an equilibrium point of the approximate continuous-time model (Eq. (46)). This is stated more formally in the following theorem, which also relates this stability result with Theorem 1.

Theorem 2 (Stability for Model CT1). *The equilibrium point* (ρ^*, V^*) *of the approximate continuous-time model* (Eq. (46)) *is asymptotically stable by the linear approximation if and only if* (C1) *holds. Recall that this condition requires*

$$F'_D(\rho^*) = -\int_{-T_1}^{T_1} |E_0(\sigma)|^2 w'_D(\sigma - \rho^*) d\sigma < 0. \tag{C1}$$

Moreover, if T_{PRI} *is sufficiently small, then stability of the equilibrium* (ρ^*, V^*) *for the approximate model* (Eq. (46)) *implies that of the equilibrium* $(\rho^*, \rho^*, V^*, V^*)$ *for the original model* (Eq. (23)).

3. GATED RANGE TRACKER WITH TWO INTEGRATORS IN THE TRACK LOOP

3.1. Discrete-Time Model DT2

The block diagrams of Figs. 1 and 2 contain a single integrator ($\frac{K}{s}$) in the track loop. A more common gated range tracker design, considered next, uses two integrators in the track loop. The needed modifications to Fig. 2 are depicted in Fig. 9, where only the dynamics from $D[k]$ to $\rho[k]$ are shown. The remainder of the system is unchanged from Fig. 2. The first design can be obtained as a special case upon setting $g_1 = 0$, $g_2 = K$ in Fig. 9. However, as noted by Hughes [11], typically g_1 is significantly greater than g_2 in practical designs using two integrators in the track loop. This provides further motivation for the analysis of this case.

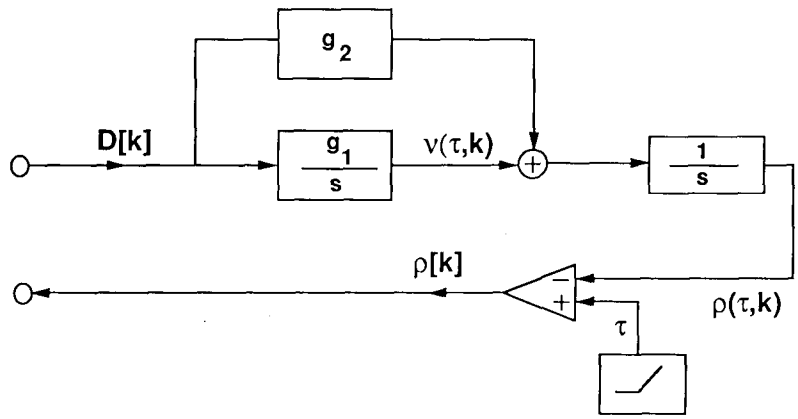

Fig. 9 — Dynamics of D and ρ in second order track loop.

Derivation of a discrete-time model for the revised block diagram, Model DT2, parallels the derivation leading to Eqs. (16) and (18) in Section 2.1. Hence only a brief summary of the derivation is necessary. Referring to Fig. 9, we have for the new dynamic variable $\nu(\tau, k)$

$$\nu(\tau, k) = \nu[k] + g_1(\tau + T_1)D[k]. \tag{48}$$

Hence

$$\nu[k+1] = \nu[k] + g_1 T_{\mathrm{PRI}} D[k]. \tag{49}$$

Also,

$$\begin{aligned}\rho(\tau, k) &= \rho[k] + \int_{-T_1}^{\tau} (\nu(\sigma, k) + g_2 D[k])\, d\sigma \\ &= \rho[k] + (\tau + T_1)(\nu[k] + g_2 D[k]) + 0.5 g_1 D[k](\tau + T_1)^2. \end{aligned} \tag{50}$$

Therefore, the variables $\rho[k]$ and $\nu[k]$ satisfy the following pair of difference equations, in which $D[k]$ is to be viewed as an input as specified in Eq. (12):

$$\rho[k+1] = \rho[k] + T_{\rm PRI}(\nu[k] + g_2\, D[k]) + 0.5 g_1\, T_{\rm PRI}^2\, D[k], \tag{51a}$$

$$\nu[k+1] = \nu[k] + g_1\, T_{\rm PRI}\, D[k]. \tag{51b}$$

Since the remaining dynamics of Fig. 2 are not altered by the introduction of an additional integrator in the track loop, a discrete-time model for Fig. 2 modified by Fig. 9 is given by

$$\rho[k+1] = \rho[k] + T_{\rm PRI}\nu[k]$$

$$+\beta^2 T_{\rm PRI}(g_2 + 0.5 g_1 T_{\rm PRI}) e^{-2V[k-1]} \int_{-T_1}^{T_1} |E(\sigma, k-1)|^2\, w_D(\sigma - \rho[k-1])\, d\sigma \tag{52a}$$

$$V[k+1] = V[k] + \frac{T_{\rm PRI}}{T_{\rm AGC}} \left(\beta^2 e^{-2V[k-1]} \int_{-T_1}^{T_1} |E(\sigma, k-1)|^2\, w_S(\sigma - \rho[k-1])\, d\sigma - 1\right) \tag{52b}$$

$$\nu[k+1] = \nu[k] + g_1 \beta^2\, T_{\rm PRI}\, e^{-2V[k-1]} \int_{-T_1}^{T_1} |E(\sigma, k-1)|^2\, w_D(\sigma - \rho[k-1])\, d\sigma. \tag{52c}$$

Note that each of Eqs. (52a) and (52b) is second order, while Eq. (52c) is first order. The model (Eq. (52)) is thus fifth order. An equivalent state space description of the model (Eq. (52)) is

Model DT2:

$$\rho[k+1] = \rho[k] + T_{\rm PRI}\, \nu[k]$$

$$+\beta^2\, T_{\rm PRI}(g_2 + 0.5 g_1\, T_{\rm PRI}) e^{-2V_d[k]} \int_{-T_1}^{T_1} |E(\sigma, k-1)|^2\, w_D(\sigma - \rho_d[k])\, d\sigma \tag{53a}$$

$$\rho_d[k+1] = \rho[k] \tag{53b}$$

$$V[k+1] = V[k] + \frac{T_{\rm PRI}}{T_{\rm AGC}} \left(\beta^2 e^{-2V_d[k]} \int_{-T_1}^{T_1} |E(\sigma, k-1)|^2\, w_S(\sigma - \rho_d[k])\, d\sigma - 1\right) \tag{53c}$$

$$V_d[k+1] = V[k] \tag{53d}$$

$$\nu[k+1] = \nu[k] + g_1\, \beta^2\, T_{\rm PRI} e^{-2V_d[k]} \int_{-T_1}^{T_1} |E(\sigma, k-1)|^2\, w_D(\sigma - \rho_d[k])\, d\sigma, \tag{53e}$$

where the delayed variables ρ_d, V_d are as defined in Eq. (17).

Equation (53) describes the dynamics of the gated range tracker for the case of two integrators in the track loop is the basis for the deterministic stability analysis to follow. This analysis parallels that of Section 2.2, which applies under the assumption of a single integrator in the track loop.

3.2. Stability Analysis of Model DT2

In this section, stability of equilibrium points of Model DT2 with periodic received signal is considered. As in Section 2.2, however, a track point of the AGC-aided range tracker need not correspond to an equilibrium

point of the state space model (Eq. (53)). Recall that a track point is any trajectory of the model for which $\rho[k] =$ a constant for all k. It is clear from Eq. (53) that constants ρ^* for which

$$\int_{-T_1}^{T_1} |E(\sigma, k)|^2 w_D(\sigma - \rho^*) d\sigma = 0 \text{ for all } k, \tag{54}$$

and corresponding trajectories of Eq. (53) for which $\rho[k] = \rho^* = \rho_d[k]$ and $\nu[k] = 0$ for all k, are track points according to this definition. Unlike the situation in Section 2, however, these need not be the only track points. Next, we focus attention on equilibrium point stability of the model of Eq. (53) under the assumption of a periodic received voltage $E(t)$.

Suppose that assumption in Eq. (20) holds, i.e., that $E(\tau, k) = E(\tau, 0) = E_0(\tau)$ for all k. Then Eq. (53) simplifies to

Model DT2 for Periodic Received Waveform:

$$\rho[k+1] = \rho[k] + T_{\text{PRI}}\, \nu[k]$$

$$+\beta^2\, T_{\text{PRI}}(g_2 + 0.5 g_1\, T_{\text{PRI}}) e^{-2V_d[k]} \int_{-T_1}^{T_1} |E_0(\sigma)|^2\, w_D(\sigma - \rho_d[k])\, d\sigma \tag{55a}$$

$$\rho_d[k+1] = \rho[k] \tag{55b}$$

$$V[k+1] = V[k] + \frac{T_{\text{PRI}}}{T_{\text{AGC}}} (\beta^2 e^{-2V_d[k]} \int_{-T_1}^{T_1} |E_0(\sigma)|^2\, w_S(\sigma - \rho_d[k])\, d\sigma - 1) \tag{55c}$$

$$V_d[k+1] = V[k] \tag{55d}$$

$$\nu[k+1] = \nu[k] + g_1\, \beta^2 T_{\text{PRI}} e^{-2V_d[k]} \int_{-T_1}^{T_1} |E_0(\sigma)|^2\, w_D(\sigma - \rho_d[k])\, d\sigma. \tag{55e}$$

To be an equilibrium point of Eq. (55), a vector $(\rho^*, \rho^*, V^*, V^*, \nu^*)$ must satisfy the following three conditions:

$$\int_{-T_1}^{T_1} |E_0(\sigma)|^2\, w_D(\sigma - \rho^*)\, d\sigma = 0 \tag{56a}$$

$$\beta^2 e^{-2V^*} \int_{-T_1}^{T_1} |E_0(\sigma)|^2\, w_S(\sigma - \rho^*)\, d\sigma - 1 = 0 \tag{56b}$$

$$\nu^* = 0. \tag{56c}$$

Denote the Jacobian matrix of the right side of Eq. (55) at such an equilibrium point by J. This matrix is given by

$$J := \begin{pmatrix} 1 & j_{12} & 0 & 0 & j_{15} \\ 1 & 0 & 0 & 0 & 0 \\ 0 & j_{32} & 1 & j_{34} & 0 \\ 0 & 0 & 1 & 0 & 0 \\ 0 & j_{52} & 0 & 0 & 1 \end{pmatrix}, \tag{57}$$

where the scalars j_{12}, j_{15}, j_{32}, j_{34}, j_{52} are defined as follows:

$$j_{12} := (g_2 + 0.5 g_1 T_{\mathrm{PRI}}) \beta^2 \, T_{\mathrm{PRI}} e^{-2V^*} F_D'(\rho^*) \tag{58a}$$

$$j_{15} := T_{\mathrm{PRI}} \tag{58b}$$

$$j_{32} := \frac{\beta^2 T_{\mathrm{PRI}} e^{-2V^*}}{T_{\mathrm{AGC}}} F_S'(\rho^*) \tag{58c}$$

$$j_{34} := -\frac{2\beta^2 T_{\mathrm{PRI}} e^{-2V^*}}{T_{\mathrm{AGC}}} F_S(\rho^*) \tag{58d}$$

$$j_{52} := \frac{g_1}{(g_2 + 0.5 g_1 T_{\mathrm{PRI}})} j_{12}, \tag{58e}$$

respectively. Here the notation F_D, F_S defined in Eq. (22) has been used. Note that j_{32} and j_{34} equal. respectively, b and c of Eq. (25). The characteristic polynomial of the matrix J is readily computed by cofactor expansion along the last row, yielding

$$\det(\lambda I - J) = -(\lambda^2 - \lambda - j_{34})[\lambda^3 - 2\lambda^2 + (1 - j_{12})\lambda + j_{12} - j_{15} j_{52}]. \tag{59}$$

Define the quadratic polynomial $q_1(\lambda)$ and the cubic polynomial $q_2(\lambda)$ as

$$q_1(\lambda) := \lambda^2 - \lambda - j_{34}, \text{ and} \tag{60a}$$

$$q_2(\lambda) := \lambda^3 - 2\lambda^2 + (1 - j_{12})\lambda + j_{12} - j_{15} j_{52}, \tag{60b}$$

respectively. Then the matrix J is stable (in the discrete-time sense) if and only if all the zeros of the polynomials q_1 and q_2 have magnitude strictly less than 1. The condition for this to hold for the polynomial $q_1(\lambda)$ has already obtained, as can be seen by noting that $q_1(\lambda) = p_1(\lambda)$ of Eq. (26). Recall that the sufficient condition is simply (C3), i.e.,

$$T_{\mathrm{AGC}} > 2T_{\mathrm{PRI}}, \tag{61}$$

and that this was obtained by invoking Lemma 1 (Jury's test for second-order systems). The analogous stability test for third-order systems, Lemma 2 below, is used in considering $q_2(\lambda)$.

Lemma 2 (Jury's Test for Third-Order Systems) *A necessary and sufficient condition for the zeros of the polynomial*

$$q(\lambda) = a_3\lambda^3 + a_2\lambda^2 + a_1\lambda + a_0 \tag{62}$$

($a_3 > 0$) *to lie within the unit circle is*

$$q(1) > 0, \tag{63a}$$

$$|a_0| < a_3, \tag{63b}$$

$$q(-1) < 0, \text{ and} \tag{63c}$$

$$|a_0^2 - a_3^2| > |a_0 a_2 - a_1 a_3|. \tag{63d}$$

Next we apply Lemma 2 to the polynomial $q_2(\lambda)$. Equation (63a) is found to assert $j_{12} < 0$, i.e.,

$$F_D'(\rho^*) < 0. \tag{64}$$

Thus Condition (C1) appears in this context as well.

Equation (63b) in this context asserts

$$|j_{12} - j_{15}j_{52}| < 1, \tag{65}$$

which is found to be tantamount to the following:

$$T_{\rm PRI}|g_2 - 0.5\,T_{\rm PRI}\,g_1| + \frac{F_S(\rho^*)}{F_D'(\rho^*)} < 0. \qquad \text{Condition (C2)}'$$

We refer to this condition as (C2)′ since it reduces to Condition (C2) for vanishing g_1.

Equation (63c) asserts

$$2j_{12} - j_{15}j_{52} < 4, \tag{66}$$

which can be seen to be automatically satisfied whenever (C1) holds.

Finally, Eq. (63d) asserts

$$|(j_{12} - j_{15}j_{52})^2 - 1| > |2j_{15}j_{52} - j_{12} - 1|. \tag{67}$$

After substitution from Eq. (58) and simplification, this is found to be equivalent to

$$|(g_2 + 1.5T_{\rm PRI}g_1)^2 \left(\frac{F_D'(\rho^*)}{F_S(\rho^*)}\right)^2 - 1|$$

$$\geq |(g_2 - 1.5T_{\rm PRI}^2 g_1)\frac{F_D'(\rho^*)}{F_S(\rho^*)} + 1|. \qquad \text{Condition (C4)}'$$

Conditions (C1), (C2)′, (C3) and (C4)′ are therefore necessary and sufficient for stability by the linear approximation of an equilibrium point of Eq. (55). This is summarized in the next theorem.

Theorem 3 (Stability for Model DT2). *Under assumption in Eq.* (20), *the equilibrium point* $(\rho^*, \rho_d^*, V^*, V_d^*, \nu^*) = (\rho^*, \rho^*, V^*, V^*, 0)$ *of Eq.* (55) *is asymptotically stable by the linear approximation if and only if conditions* (C1), (C2)′ (C3) *and* (C4)′ *above hold.*

3.3. Approximate Continuous-Time Model CT2

Model CT2

The fifth-order model Eq. (53), Model DT2, may be approximated by a third-order continuous-time model, if $T_{\rm PRI}$ is small. The derivation of the model is nearly identical to the derivation in Section 2.4, and so it is omitted. The notation is also clear given the notation of Section 2.4. The resulting continuous-time model is

Model CT2:

$$\frac{d\rho(t)}{dt} = \nu(t) + \beta^2(g_2 + 0.5g_1T_{\rm PRI})e^{-2V(t)}$$

$$\times \int_{-T_1}^{T_1} \left| E\left(\sigma - T_{\rm PRI} + \left[\frac{t}{T_{\rm PRI}}\right] T_{\rm PRI}\right)\right|^2 w_D(\sigma - \rho(t))d\sigma, \tag{68a}$$

$$T_{\mathrm{AGC}}\frac{dV(t)}{dt} = \beta^2 e^{-2V(t)} \int_{-T_1}^{T_1} \left| E\left(\sigma - T_{\mathrm{PRI}} + \left[\frac{t}{T_{\mathrm{PRI}}}\right] T_{\mathrm{PRI}}\right)\right|^2 w_S(\sigma - \rho(t))d\sigma - 1, \tag{68b}$$

$$\frac{d\nu(t)}{dt} = g_1\beta^2 e^{-2V(t)} \int_{-T_1}^{T_1} \left| E\left(\sigma - T_{\mathrm{PRI}} + \left[\frac{t}{T_{\mathrm{PRI}}}\right] T_{\mathrm{PRI}}\right)\right|^2 w_D(\sigma - \rho(t))d\sigma. \tag{68c}$$

We refer to this as Model CT2.

If the received signal is periodic with period T_{PRI}, Eq. (68) simplifies to:

Model CT2 for Periodic Received Waveform:

$$\frac{d\rho(t)}{dt} = \nu(t) + \beta^2(g_2 + 0.5g_1T_{\mathrm{PRI}})e^{-2V(t)} \int_{-T_1}^{T_1} |E_0(\sigma)|^2 w_D(\sigma - \rho(t))\, d\sigma, \tag{69a}$$

$$T_{\mathrm{AGC}}\frac{dV(t)}{dt} = \beta^2 e^{-2V(t)} \int_{-T_1}^{T_1} |E_0(\sigma)|^2 w_S(\sigma - \rho(t))\, d\sigma - 1, \tag{69b}$$

$$\frac{d\nu(t)}{dt} = g_1\beta^2 e^{-2V(t)} \int_{-T_1}^{T_1} |E_0(\sigma)|^2 w_D(\sigma - \rho(t))\, d\sigma. \tag{69c}$$

Equation (69) should be compared to Eq. (46), which applies under the analogous assumptions for the case of a single integrator in the track loop.

Stability Analysis of Model CT2

The Jacobian matrix J of Eq. (69) evaluated at an equilibrium point $(\rho^*, V^*, \nu^* = 0)$ is given by

$$J = \begin{pmatrix} j_{11} & 0 & 1 \\ j_{21} & j_{22} & 0 \\ j_{31} & 0 & 0 \end{pmatrix}, \tag{70}$$

where

$$j_{11} := (g_2 + 0.5g_1T_{\mathrm{PRI}})\beta^2 e^{-2V^*} F_D'(\rho^*) \tag{71a}$$

$$j_{21} := -\frac{\beta^2 e^{-2V^*}}{T_{\mathrm{AGC}}} F_S'(\rho^*) \tag{71b}$$

$$j_{22} := -\frac{2\beta^2 e^{-2V^*}}{T_{\mathrm{AGC}}} F_S(\rho^*) \tag{71c}$$

$$j_{31} := g_1\beta^2 e^{-2V^*} F_D'(\rho^*). \tag{71d}$$

The characteristic polynomial of J is, after some simplification, found to be

$$\lambda^3 + \left(\frac{2}{T_{\mathrm{AGC}}} - (g_2 + 0.5g_1\, T_{\mathrm{PRI}})\, \frac{F_D'(\rho^*)}{F_S(\rho^*)}\right)\lambda^2$$

$$+ \left(g_1 - \frac{2}{T_{\mathrm{AGC}}}(g_2 + 0.5g_1T_{\mathrm{PRI}})\right)\frac{F_D'(\rho^*)}{F_S(\rho^*)}\lambda$$

$$-\frac{2g_1}{T_{\mathrm{AGC}}}\frac{F_D'(\rho^*)}{F_S(\rho^*)}. \tag{72}.$$

Condition (C1) is clearly necessary for all the coefficients in this polynomial to be positive, which is the first requirement for a cubic polynomial to be stable in the continuous-time sense (entailing that all the zeros have strictly negative real parts). The second requirement, for an arbitrary polynomial with real coefficients $\lambda^3 + a_2\lambda^2 + a_1\lambda + a_0$, is that $a_1 a_2 > a_0$. For Eq. (72), this is automatically satisfied for any $g_1 > 0$, given that (C1) holds. Therefore, we arrive at the following result.

Theorem 4 (Stability for Model CT2). *The equilibrium point* $(\rho^*, V^*, 0)$ *of the approximate continuous-time model* Eq. (69) *is asymptotically stable by the linear approximation if and only if* (C1) *holds there.*

4. CONCLUSIONS

A new class of models has been presented for AGC-aided gated range trackers. The models are nonlinear and allow for statistical variation of the received signal. The utility of the models has been demonstrated by deriving, for each model, criteria for deterministic stability of track points within a range gate. These criteria may be used to determine whether or not the range tracker can converge on a target, or possibly on an artificial centroid target. The stability of a centroid track point and the resolving power of a range tracker were analyzed in an example involving two closely spaced identical point targets. The result was considered in the light of a previous conclusion based on ambiguity functions.

Extensions of the work in at least two directions are important. First, the models should be analyzed under stochastic target return conditions. That is, the stochastic stability of track point should be studied. Here, the signal E is a stochastic process, the models become stochastic difference or differential equations, and pathwise analysis must be replaced by a statistical description of tracker behavior. A second extension of the work would be concerned with the interaction between tracking in angle and range, and would begin by expanding the models of this paper to account for the angle tracking servo-loops. Note that several authors have considered angle tracking performance in multiple target conditions using dynamical modeling of the angle tracking servo-loops and stability analysis [12, 13, 14].

ACKNOWLEDGMENT

The authors are grateful to Dr. J. Lawrence of the Naval Research Laboratory for helpful discussions.

REFERENCES

1. R.J. Schlesinger, *Principles of Electronic Warfare* (Prentice-Hall, Englewood-Cliffs, NJ, 1961).

2. J.A. Stuller, "Generalized Likelihood Signal Resolution," *IEEE Trans. Inf. Theory*, **IT-21**, 276-282 (1973).

3. P.M. Woodward, *Probability and Information Theory with Applications to Radar* (Pergamon Press, New York, 1955).

4. H. Urkowitz, C.A. Hauer, and J.F. Koval, "Generalized Resolution in Radar Systems," *Proc. IRE* **50**, 2093-2105 (1962).

5. E.H. Ehling, (ed.), *Range Instrumentation,* (Prentice-Hall, Englewood Cliffs, NJ, 1967).

6. I.N. Amiantov and V.I. Tikhonov, "The Effect of Fluctuations on the Operation of an Automatic Range Finder," pp. 209-219 in *Non-Linear Transformations of Stochastic Processes*, P.I. Kuznetsov, R.L. Stratonovich, and V.I. Tikhonov, (eds.) (English Edition, Pergamon Press, Oxford, 1965). (Original article in *Avtomatika i telemekhanika*, Vol. 19, 1958).

7. A.S. Locke, (Principal Author), *Guidance*, Principles of Guided Missile Design Series (D. Van Nostrand Co, Princeton, NJ, 1955).

8. D.P. Lindorff, *Theory of Sampled-Data Control Systems* (John Wiley and Sons, New York, 1965).

9. A. Golden, "Radar Separation of Closely Spaced Targets," *IEEE Spectrum* **3**, 94-98 (1966).

10. W.S. Burdic, *Radar Signal Analysis* (Prentice-Hall, Englewood Cliffs, NJ, 1968).

11. R.S. Hughes, "A Practical Approach to the Analysis and Design of Zero Velocity Error Range Trackers," NWC-TP-5566, Naval Weapons Center, China Lake, CA (Dec. 1973).

12. P.R. Dax, "Accurate Tracking of Low Elevation Targets over the Sea with a Monopulse Radar," pp. 160-165 in *Radar - Present and Future*, IEE Conf. Publ. No. 105, London (1973).

13. M.R. Ducoff, "Closed-loop Angle Tracking of Unresolved Targets," pp. 432-437 in *Record of the IEEE International Radar Conference*, Arlington, VA (1980).

14. T. Endo and T. Suzuki, "Influence of an Interfering Second Target on a Certain Amplitude-comparison Monopulse Radar System," *Electron. Commun. Japan* **67-B**, 66-75 (1984).